arXiv:hep-ex/0011081v2   8 Dec 2000

# Measurement of open beauty production in photoproduction at HERA

ZEUS Collaboration

**Abstract**

The production and semi-leptonic decay of heavy quarks have been studied in the photoproduction process $e^+ p \rightarrow e^+ + \mathrm{dijet} + e^- + X$ with the ZEUS detector at HERA using an integrated luminosity of 38.5 pb$^{-1}$. Events with photon-proton centre-of-mass energies, $W_{\gamma p}$, between 134 and 269 GeV and a photon virtuality, $Q^2$, less than 1 GeV$^2$ were selected requiring at least two jets of transverse energy $E_T^{\mathrm{jet1(2)}} > 7(6)$ GeV and an electron in the final state. The electrons were identified by employing the ionisation energy loss measurement. The contribution of beauty quarks was determined using the transverse momentum of the electron relative to the axis of the closest jet, $p_T^{\mathrm{rel}}$. The data, after background subtraction, were fit with a Monte Carlo simulation including beauty and charm decays. The measured beauty cross section was extrapolated to the parton level with the $b$ quark restricted to the region of transverse momentum $p_T^b > p_T^{\mathrm{min}} = 5$ GeV and pseudorapidity $|\eta^b| < 2$. The extrapolated cross section is $1.6 \pm 0.4 \, (stat.)^{+0.3}_{-0.5}(syst.)^{+0.2}_{-0.4}(ext.)$ nb. The result is compared to a perturbative QCD calculation performed to next-to-leading order.

# The ZEUS Collaboration

J. Breitweg, S. Chekanov, M. Derrick, D. Krakauer, S. Magill, B. Musgrave, A. Pellegrino, J. Repond, R. Stanek, R. Yoshida
*Argonne National Laboratory, Argonne, IL, USA [p]*

M.C.K. Mattingly
*Andrews University, Berrien Springs, MI, USA*

P. Antonioli, G. Bari, M. Basile, L. Bellagamba, D. Boscherini[1], A. Bruni, G. Bruni, G. Cara Romeo, L. Cifarelli[2], F. Cindolo, A. Contin, M. Corradi, S. De Pasquale, P. Giusti, G. Iacobucci, G. Levi, A. Margotti, T. Massam, R. Nania, F. Palmonari, A. Pesci, G. Sartorelli, A. Zichichi
*University and INFN Bologna, Bologna, Italy [f]*

G. Aghuzumtsyan, C. Amelung[3], I. Brock, K. Coböken[4], S. Goers, H. Hartmann, K. Heinloth[5], E. Hilger, P. Irrgang, H.-P. Jakob, A. Kappes[6], U.F. Katz, R. Kerger, O. Kind, E. Paul, J. Rautenberg, H. Schnurbusch, A. Stifutkin, J. Tandler, K.C. Voss, A. Weber, H. Wieber
*Physikalisches Institut der Universität Bonn, Bonn, Germany [c]*

D.S. Bailey, O. Barret, N.H. Brook[7], J.E. Cole, B. Foster[1], G.P. Heath, H.F. Heath, S. Robins, E. Rodrigues[8], J. Scott, R.J. Tapper
*H.H. Wills Physics Laboratory, University of Bristol, Bristol, U.K. [o]*

M. Capua, A. Mastroberardino, M. Schioppa, G. Susinno
*Calabria University, Physics Dept.and INFN, Cosenza, Italy [f]*

H.Y. Jeoung, J.Y. Kim, J.H. Lee, I.T. Lim, K.J. Ma, M.Y. Pac[9]
*Chonnam National University, Kwangju, Korea [h]*

A. Caldwell, W. Liu, X. Liu, B. Mellado, S. Paganis, S. Sampson, W.B. Schmidke, F. Sciulli
*Columbia University, Nevis Labs., Irvington on Hudson, N.Y., USA [q]*

J. Chwastowski, A. Eskreys, J. Figiel, K. Klimek, K. Olkiewicz, K. Piotrzkowski[3], M.B. Przybycień, P. Stopa, L. Zawiejski
*Inst. of Nuclear Physics, Cracow, Poland [j]*

B. Bednarek, K. Jeleń, D. Kisielewska, A.M. Kowal, T. Kowalski, M. Przybycień, E. Rulikowska-Zarębska, L. Suszycki, D. Szuba
*Faculty of Physics and Nuclear Techniques, Academy of Mining and Metallurgy, Cracow, Poland [j]*

A. Kotański
*Jagellonian Univ., Dept. of Physics, Cracow, Poland [k]*

L.A.T. Bauerdick, U. Behrens, J.K. Bienlein, K. Borras, V. Chiochia, J. Crittenden[10], D. Dannheim, K. Desler, G. Drews, A. Fox-Murphy, U. Fricke, F. Goebel, P. Göttlicher, R. Graciani, T. Haas, W. Hain, G.F. Hartner, K. Hebbel, S. Hillert, W. Koch[11]†, U. Kötz, H. Kowalski, H. Labes, B. Löhr, R. Mankel, J. Martens, M. Martínez, M. Milite, M. Moritz, D. Notz, M.C. Petrucci, A. Polini, M. Rohde[5], A.A. Savin, U. Schneekloth, F. Selonke, M. Sievers[12], S. Stonjek, G. Wolf, U. Wollmer, C. Youngman, W. Zeuner
*Deutsches Elektronen-Synchrotron DESY, Hamburg, Germany*

C. Coldewey, A. Lopez-Duran Viani, A. Meyer, S. Schlenstedt, P.B. Straub
*DESY Zeuthen, Zeuthen, Germany*

G. Barbagli, E. Gallo, A. Parenti, P. G. Pelfer
*University and INFN, Florence, Italy [f]*

A. Bamberger, A. Benen, N. Coppola, S. Eisenhardt[13], P. Markun, H. Raach, S. Wölfle
*Fakultät für Physik der Universität Freiburg i.Br., Freiburg i.Br., Germany [c]*

P.J. Bussey, M. Bell, A.T. Doyle, C. Glasman, S.W. Lee[14], A. Lupi, N. Macdonald, G.J. McCance,
D.H. Saxon, L.E. Sinclair, I.O. Skillicorn, R. Waugh
*Dept. of Physics and Astronomy, University of Glasgow, Glasgow, U.K. [o]*

B. Bodmann, N. Gendner, U. Holm, H. Salehi, K. Wick, A. Yildirim
*Hamburg University, I. Institute of Exp. Physics, Hamburg, Germany [c]*

T. Carli, A. Garfagnini, A. Geiser, I. Gialas[15], D. Kçira[16], R. Klanner, E. Lohrmann
*Hamburg University, II. Institute of Exp. Physics, Hamburg, Germany [c]*

R. Gonçalo[8], K.R. Long, D.B. Miller, A.D. Tapper, R. Walker
*Imperial College London, High Energy Nuclear Physics Group, London, U.K. [o]*

P. Cloth, D. Filges
*Forschungszentrum Jülich, Institut für Kernphysik, Jülich, Germany*

T. Ishii, M. Kuze, K. Nagano, K. Tokushuku[17], S. Yamada, Y. Yamazaki
*Institute of Particle and Nuclear Studies, KEK, Tsukuba, Japan [g]*

A.N. Barakbaev, E.G. Boos, N.S. Pokrovskiy, B.O. Zhautykov
*Institute of Physics and Technology of Ministry of Education and Science of Kazakhstan, Almaty, Kazakhstan*

S.H. Ahn, S.B. Lee, S.K. Park
*Korea University, Seoul, Korea [h]*

H. Lim[14], D. Son
*Kyungpook National University, Taegu, Korea [h]*

F. Barreiro, G. García, O. González, L. Labarga, J. del Peso, I. Redondo[18], J. Terrón, M. Vázquez
*Univer. Autónoma Madrid, Depto de Física Teórica, Madrid, Spain [n]*

M. Barbi, F. Corriveau, S. Padhi, D.G. Stairs, M. Wing
*McGill University, Dept. of Physics, Montréal, Québec, Canada [a], [b]*

T. Tsurugai
*Meiji Gakuin University, Faculty of General Education, Yokohama, Japan*

A. Antonov, V. Bashkirov[19], M. Danilov, B.A. Dolgoshein, D. Gladkov, V. Sosnovtsev, S. Suchkov
*Moscow Engineering Physics Institute, Moscow, Russia [l]*

R.K. Dementiev, P.F. Ermolov, Yu.A. Golubkov, I.I. Katkov, L.A. Khein, N.A. Korotkova,
I.A. Korzhavina, V.A. Kuzmin, O.Yu. Lukina, A.S. Proskuryakov, L.M. Shcheglova, A.N. Solomin,
N.N. Vlasov, S.A. Zotkin
*Moscow State University, Institute of Nuclear Physics, Moscow, Russia [m]*

C. Bokel, M. Botje, N. Brümmer, J. Engelen, S. Grijpink, E. Koffeman, P. Kooijman, S. Schagen,
A. van Sighem, E. Tassi, H. Tiecke, N. Tuning, J.J. Velthuis, J. Vossebeld, L. Wiggers, E. de Wolf
*NIKHEF and University of Amsterdam, Amsterdam, Netherlands [i]*

B. Bylsma, L.S. Durkin, J. Gilmore, C.M. Ginsburg, C.L. Kim, T.Y. Ling
*Ohio State University, Physics Department, Columbus, Ohio, USA [p]*

S. Boogert, A.M. Cooper-Sarkar, R.C.E. Devenish, J. Große-Knetter[20], T. Matsushita, O. Ruske,
M.R. Sutton, R. Walczak
*Department of Physics, University of Oxford, Oxford U.K. [o]*

A. Bertolin, R. Brugnera, R. Carlin, F. Dal Corso, S. Dusini, S. Limentani, A. Longhin, M. Posocco,
L. Stanco, M. Turcato
*Dipartimento di Fisica dell' Università and INFN, Padova, Italy [f]*

L. Adamczyk[21], L. Iannotti[21], B.Y. Oh, J.R. Okrasiński, P.R.B. Saull[21], W.S. Toothacker[11]†,
J.J. Whitmore
*Pennsylvania State University, Dept. of Physics, University Park, PA, USA [q]*

Y. Iga
*Polytechnic University, Sagamihara, Japan [g]*

G. D'Agostini, G. Marini, A. Nigro
*Dipartimento di Fisica, Univ. 'La Sapienza' and INFN, Rome, Italy [f]*

C. Cormack, J.C. Hart, N.A. McCubbin, T.P. Shah
*Rutherford Appleton Laboratory, Chilton, Didcot, Oxon, U.K. [o]*

D. Epperson, C. Heusch, H.F.-W. Sadrozinski, A. Seiden, R. Wichmann, D.C. Williams
*University of California, Santa Cruz, CA, USA [p]*

I.H. Park
*Seoul National University, Seoul, Korea*

N. Pavel
*Fachbereich Physik der Universität-Gesamthochschule Siegen, Germany [c]*

H. Abramowicz[22], S. Dagan[23], A. Gabareen, S. Kananov[23], A. Kreisel, A. Levy[23]
*Raymond and Beverly Sackler Faculty of Exact Sciences, School of Physics, Tel-Aviv University,
Tel-Aviv, Israel [e]*

T. Abe, T. Fusayasu, T. Kohno, K. Umemori, T. Yamashita
*Department of Physics, University of Tokyo, Tokyo, Japan [g]*

R. Hamatsu, T. Hirose, M. Inuzuka, S. Kitamura[24], K. Matsuzawa, T. Nishimura
*Tokyo Metropolitan University, Dept. of Physics, Tokyo, Japan [g]*

M. Arneodo[25], N. Cartiglia, R. Cirio, M. Costa, M.I. Ferrero, S. Maselli, V. Monaco, C. Peroni,
M. Ruspa, R. Sacchi, A. Solano, A. Staiano
*Università di Torino, Dipartimento di Fisica Sperimentale and INFN, Torino, Italy [f]*

D.C. Bailey, C.-P. Fagerstroem, R. Galea, T. Koop, G.M. Levman, J.F. Martin, A. Mirea, A. Sa-
betfakhri
*University of Toronto, Dept. of Physics, Toronto, Ont., Canada [a]*

J.M. Butterworth, C. Gwenlan, M.E. Hayes, E.A. Heaphy, T.W. Jones, J.B. Lane, B.J. West
*University College London, Physics and Astronomy Dept., London, U.K. [o]*

J. Ciborowski, R. Ciesielski, G. Grzelak, R.J. Nowak, J.M. Pawlak, R. Pawlak, B. Smalska[26],
T. Tymieniecka, A.K. Wróblewski, J.A. Zakrzewski, A.F. Żarnecki
*Warsaw University, Institute of Experimental Physics, Warsaw, Poland [j]*

III

M. Adamus, T. Gadaj
*Institute for Nuclear Studies, Warsaw, Poland [j]*

O. Deppe, Y. Eisenberg, L.K. Gladilin[27], D. Hochman, U. Karshon[23]
*Weizmann Institute, Department of Particle Physics, Rehovot, Israel [d]*

W.F. Badgett, D. Chapin, R. Cross, C. Foudas, S. Mattingly, D.D. Reeder, W.H. Smith, A. Vaiciulis[28],
T. Wildschek, M. Wodarczyk
*University of Wisconsin, Dept. of Physics, Madison, WI, USA [p]*

A. Deshpande, S. Dhawan, V.W. Hughes
*Yale University, Department of Physics, New Haven, CT, USA [p]*

S. Bhadra, C.D. Catterall, W.R. Frisken, R. Hall-Wilton, M. Khakzad, S. Menary
*York University, Dept. of Physics, Toronto, Ont., Canada [a]*

# 1  Introduction

High-energy collisions between a quasi-real photon, emitted by an incoming positron, and a proton can lead to the production of heavy quarks. Such processes allow a test of perturbative QCD (pQCD) since the mass of the heavy quark provides a hard scale.

Measurements of charm production in $\gamma p$ collisions at HERA have been made [1, 2] by reconstructing $D^{*\pm}(2010)$ mesons. The cross sections generally lie above the pQCD predictions. The study of beauty production is important since the heavier $b$-quark mass provides a harder scale, thus making pQCD calculations more reliable. However, the higher mass and the smaller electric charge of the $b$-quark lead to cross sections in $ep$ collisions that are typically two orders of magnitude smaller than that of charm. The first measurement of the cross section for beauty photoproduction has been performed using events with a muon and two jets [3] and is higher than pQCD expectations. In $p\bar{p}$ interactions the measured beauty cross sections [4, 5, 6] significantly exceed the predictions.

This paper presents a measurement of beauty production in photon-proton collisions using a sample of events each containing two jets and a candidate for the electron from a semi-leptonic decay of a heavy quark:

$$e^+ p \rightarrow e^+(\gamma)\, p \rightarrow e^+ + \text{dijet} + e^- + X. \tag{1}$$

Reaction (1) is isolated by statistically subtracting the hadronic background from an electron-enriched sample of events selected using measurements of the ionisation energy loss of charged particles.

# 2  Experimental conditions

The data used were collected by the ZEUS experiment during the 1996 and 1997 running periods, when HERA operated with protons of energy $E_p = 820$ GeV and positrons of energy $E_e = 27.5$ GeV. The data for this study correspond to an integrated luminosity of $38.5 \pm 0.6$ pb$^{-1}$. A detailed description of the ZEUS detector can be found elsewhere [7, 8]. A brief outline of the components that are most relevant for this analysis is given below.

Charged particles are measured in the central tracking detector (CTD) [9], which operates in a magnetic field of 1.43 T provided by a thin superconducting coil. The CTD consists of 72 cylindrical drift chamber layers, organised in 9 superlayers covering the polar angle[1] region $15° < \theta < 164°$. The transverse-momentum resolution for full-length tracks is $\sigma_{p_T}/p_T = 0.0058 p_T \oplus 0.0065 \oplus 0.0014/p_T$ with $p_T$ in GeV. The energy loss of charged particles per unit track length, $dE/dx$, is also measured in the CTD [10].

The high-resolution uranium-scintillator calorimeter (CAL) [11] consists of three parts: the forward (FCAL), the barrel (BCAL) and the rear (RCAL) calorimeters. Each part is subdivided transversely into towers and longitudinally into one electromagnetic (EMC) and either one (in RCAL) or two (in BCAL and FCAL) hadronic sections (HAC). The smallest subdivision of the calorimeter is called a cell. The electromagnetic section of the BCAL (BEMC) consists of cells of $\sim$20 cm length azimuthally and mean width 5.5 cm in the $Z$ direction at a mean radius of $\sim$1.3 m from the beam

---

[1]The ZEUS co-ordinates form a right-handed system with positive-$Z$ in the proton beam direction and a horizontal $X$-axis pointing towards the centre of HERA. The nominal interaction point is at $X = Y = Z = 0$.

line. These cells have a projective geometry as viewed from the interaction point. The CAL relative energy resolutions, as measured under test beam conditions are $18\%/\sqrt{E}$ for electrons and $35\%/\sqrt{E}$ for hadrons ($E$ in GeV). Energy deposits in the CAL were used to measure the transverse energy and direction of jets. Cell clusters were also formed, which were then used to aid in the identification of electrons for the cross-section measurements.

The luminosity was measured from the rate of the bremsstrahlung process $e^+p \rightarrow e^+\gamma p$, where the photon was measured in a lead-scintillator calorimeter [12] located at $Z = -107$ m.

A three-level trigger system was used to select events online [8, 13]. At the third level, a cone algorithm was applied to the calorimeter cells and jets were reconstructed using the deposited energy and positions of the CAL cells. Events with at least two jets, each of which satisfied the requirements that the transverse energy exceeded 4 GeV and pseudorapidity was less than 2.5, were accepted.

# 3  Analysis

## 3.1  Offline cuts and event selection

To suppress backgrounds from beam-gas interactions, cosmic rays and from deep inelastic scattering, the following cuts were applied:

- neutral current deep inelastic scattering events with a well measured scattered positron candidate in the CAL were removed by cutting on the inelasticity, $y$, [14] which is the fraction of the electron energy carried by the photon in the proton rest frame. For an incoming positron of energy $E_e$, $y$ is estimated from $y_e = 1 - \frac{E'_e}{2E_e}(1 - \cos\theta'_e)$ where $E'_e$ and $\theta'_e$ are the energy and polar angle of the outgoing positron.

- the requirement $0.2 < y_{\mathrm{JB}} < 0.8$ was imposed, where $y_{\mathrm{JB}}$ is the estimator of $y$ measured from the CAL energy deposits according to the Jacquet-Blondel method [15]. The cut was imposed after correction for energy loss due to inactive material in the detector. This range in $y_{\mathrm{JB}}$ corresponds to a photon-proton centre-of-mass energy, $W_{\gamma p}$ from 134 to 269 GeV.

These cuts restrict the photon virtuality, $Q^2$, to less than 1 GeV$^2$. The median value of about $10^{-3}$ GeV$^2$ was estimated from a Monte Carlo (MC) simulation.

Jets were reconstructed using the KTCLUS [16] finder in its "inclusive" mode [17]. KTCLUS is a clustering algorithm which combines objects with small relative transverse energy into jets. The objects input to the jet algorithm may be hadrons in a simulated hadronic final state, the final-state partons of a pQCD calculation, or energy deposits in the CAL. After applying the KTCLUS jet algorithm to the calorimeter cells, the jet transverse energy was corrected for energy loss due to inactive material in the detector as a function of $\eta^{\mathrm{jet}}_{\mathrm{CAL}}$ and $E^{\mathrm{jet}}_{T,\mathrm{CAL}}$ as described in a previous ZEUS publication [13]. After these corrections, all jets with $|\eta^{\mathrm{jet}}| < 2.4$ and a transverse energy $E^{\mathrm{jet}}_T > 6$ GeV were kept. Each event was required to have at least two jets satisfying these criteria, with at least one jet having $E^{\mathrm{jet}}_T$ of more than 7 GeV.

## 3.2 Electron finding

Electrons were identified in the CTD from the $dE/dx$ of charged tracks, using a method of statistical subtraction [18, 19]. Two samples of tracks were defined using information from the CAL: the first enriched with electrons with a background of hadrons (electron-enriched sample) and the second containing only hadrons (hadronic sample). The two samples were obtained by considering clusters in the calorimeter and performing a selection on the basis of the energies deposited in the EMC and HAC sections of the CAL. The CAL clusters matched to tracks were required to have a distance of closest approach, $d$, to the track of less than 20 cm.

### 3.2.1 Electron-enriched and hadronic samples

Using the matched track-cluster pairs, the electron-enriched and hadronic samples were defined by a cut on the ratio of electromagnetic energy, $E_{EMC}$, to total energy, $E_{TOT}$, of the clusters. The electron-enriched sample[2] was required to have $E_{EMC}/E_{TOT} > 0.9$, while the hadronic sample was required to have $E_{EMC}/E_{TOT} < 0.4$, with a further requirement on the energy deposited in the hadronic section of the calorimeter, $E_{HAC} > 0.3$ GeV. These requirements on the hadronic sample efficiently rejected electrons; the residual contamination from electrons was estimated from photons converting into electron-positron pairs, reconstructed as described below, to be less than 0.03%. The selection criteria for the electron-enriched sample were 75% efficient for tagging electrons, as determined from the same sample of photon conversions.

### 3.2.2 Measurement of $dE/dx$

Charged particles traversing the CTD lose energy primarily by ionising gas in the detector. In order to estimate $dE/dx$ for each track, the truncated mean of the anode-wire pulse heights was calculated, which removes the lowest 10% and at least the highest 30% depending on the number of saturated hits. For electrons traversing all superlayers, implying a maximum of 72 possible hits, on average 32 pulse-height measurements were retained.

Since the CTD operates at ambient atmospheric pressure, the $dE/dx$ calibration was changing throughout the measurement period. The measured $dE/dx$ values were corrected [19] by normalising to the average $dE/dx$ for tracks around the region of minimum ionisation for pions, $0.3 < p^{trk} < 0.4$ GeV, where the separation from other types of particles is particularly good. Henceforth $dE/dx$ is quoted in units of *mips* - minimum ionising particles.

The measured $dE/dx$ value also depends on the polar angle. There is a trivial $1/\cos\theta$ dependence due to the path length which is corrected for in the subsequent plots. In addition, there is a dependence on $\theta$ arising from the reduction in gain that occurs through screening of ions in the avalanche. This effect was studied using a sample of electrons originating from photons which converted in the beam-pipe via the $\gamma \rightarrow e^+e^-$ process. The candidate tracks were initially selected

---

[2]Since the value of $dE/dx$ is particle dependent, the relative fractions of pions, kaons and protons determine the background in the electron- or positron-enriched sample. This background can only be estimated using the hadronic sample. Monte Carlo studies showed that, for positively charged particles, the $\pi/(K, p)$ ratio of the hadronic sample was markedly different to that of the hadronic background in the positron-enriched sample. This effect is caused by the differing cross sections for positive, compared to negative, low-energy pions, kaons and protons interacting with nuclei [20] Therefore, since a reliable statistical subtraction was not possible, positrons were not considered further in this analysis.

on the basis of their distance of closest approach, vertex position and invariant mass. The quality factor, $D = \sqrt{(\Delta xy/\sigma_{xy})^2 + (\Delta\theta/\sigma_\theta)^2}$, was calculated, where $\Delta xy$ is the separation of the tracks in two dimensions at the point at which their tangents are parallel, $\Delta\theta$ is the difference in polar angles and $\sigma_{xy}$ and $\sigma_\theta$ are the respective resolutions [18]. The distribution of the quantity $D$ is shown in Fig. 1a, which demonstrates that real conversions, with net charge zero, tend to have lower values of $D$ and as shown in Fig. 1b, low invariant masses of the electron-positron pair, $M_{e^+e^-}$. To achieve a pure sample of electrons, relatively hard cuts of $D < 5$ and $M_{e^+e^-} < 0.025$ GeV were applied. Electron-positron candidates of net-zero and net-two units of charge were considered and the two subtracted as shown in Fig. 2a. The $dE/dx$ distribution for the sample of clean electrons has a roughly Gaussian shape centred about $dE/dx \sim 1.4$ mips with width 0.14 mips, corresponding to a resolution of $\sim 10\%$. Figure 2b shows that the $dE/dx$ value exhibits a strong dependence on the polar angle, $\theta^{\mathrm{trk}}$, as expected from the space-charge effect [21]. The value of $dE/dx$ at $\theta^{\mathrm{trk}} = \pi/2$ is about 10% lower than the most forward and backward values in the range of $\theta^{\mathrm{trk}}$ considered. Using this sample of electrons, correction factors were obtained which depend on $\theta^{\mathrm{trk}}$. The $dE/dx$ for electrons was corrected such that the mean was 1.4 mips.

### 3.2.3 Tracking requirements

Negatively charged tracks with a transverse momentum relative to the $ep$ beam axis, $p_T^{\mathrm{trk}}$, greater than 1.6 GeV were selected. Electron candidates were restricted to the central region of the detector, $|\eta^{\mathrm{trk}}| < 1.1$, corresponding to $0.64 < \theta^{\mathrm{trk}} < 2.50$ radians, where the resolution in $dE/dx$ is constant to within 10%. A small slice in $\eta^{\mathrm{trk}}$ was removed from the analysis, corresponding to the region in which tracks were matched to clusters where the BCAL and RCAL meet, where CAL clusters were not well reconstructed. Figure 3 shows that for $1.6 < p_T^{\mathrm{trk}} < 10$ GeV, all hadrons have an average $dE/dx$ value well below that of electrons, thus allowing the separation of electrons from hadrons.

### 3.2.4 Background electrons from converting photons

The major source of background to electrons from semi-leptonic decays of heavy quarks (prompt electrons) comes from photon conversions in the detector. Electron-positron pairs were initially selected as discussed in Section 3.2.2. A loose cut of $D < 15$ was chosen.

Tracks above a momentum of 0.2 GeV were reconstructed with an efficiency of greater than 95%. The number of potential conversion candidates not identified after this cut because the electron-positron pair was asymmetric in momentum was determined from a calculation of pair production [22] rather than by relying on a MC model. After the $p^{\mathrm{trk}} > 0.2$ GeV cut on the positron candidate was imposed, good agreement was seen between data and expectation for the shape of $E_{e^-}/E_\gamma$, the fraction of the photon's energy carried by the electron, as shown in Fig. 4. This demonstrates that the identified electron-positron candidates originated from photon conversions. The requirement for the positron's momentum, $p^{e^+} > 0.2$ GeV, was then removed in the calculation and the ratio, $\epsilon(E_\gamma) = N(p_T^{e^-} > 1.6 \text{ GeV}, \ p^{e^+} > 0.2 \text{ GeV})/N(p_T^{e^-} > 1.6 \text{ GeV})$ of the two theoretical predictions (the solid and dashed curves in Fig. 4) determined, where $N$ is the number of photon conversions. The efficiency, $\epsilon$, averaged over the photon energy was found to be 83%.

The overall efficiency for tagging the background due to electrons from photon conversions was determined from MC simulations. This was achieved by performing the analysis procedure with an inclusive MC conversion sample but demanding no prompt electron. The number of electrons

found by the analysis procedure, together with the number of electrons identified as coming from converting photons by the above two steps, was determined. The ratio of the number of identified conversion candidates to the total number of candidates passing the analysis cuts was $90 \pm 3\%$ which in combination with $\epsilon = 83\%$, leads to an overall efficiency for the identification of conversion candidates of $75 \pm 3\%$.

### 3.2.5 Electrons from Dalitz decays, $\pi^0 \rightarrow e^+ e^- \gamma$

A substantial background is produced by Dalitz decays, $\pi^0 \rightarrow e^+ e^- \gamma$. To remove this background, all tracks in the electron-enriched sample that were not identified as coming from conversions, were combined with tracks of positive charge and the invariant mass formed. The positively charged tracks were required to have originated from the primary vertex, to have passed through at least the first three superlayers of the CTD and to have $p_T^{\text{trk}} > 0.1$ GeV. Since MC simulations showed that no fully reconstructed Dalitz decays survived a cut of $M_{e^+e^-} > 0.2$ GeV, an electron candidate was removed if any combination failed this cut. The overall rejection efficiency was $84 \pm 2\%$.

### 3.2.6 Electron signal

In order to subtract statistically the hadronic background from the electron-enriched sample, the dependence of the measured $dE/dx$ on momentum and polar angle must be taken into account. As the $p$ and $\theta$ distributions for the electron-enriched and hadronic samples differ, subtraction of the hadronic background was carried out by reweighting the hadronic sample to give the same distribution as the hadronic background in the electron-enriched sample. This was achieved by binning the distributions in transverse momentum and pseudorapidity and normalising the hadronic sample to the electron-enriched sample in the region $0.5 < dE/dx < 1.1$ mips. In this analysis, 64 bins, with eight divisions in $p_T^{\text{trk}}$ and eight in $\eta^{\text{trk}}$, were used.

Figure 5a shows the $dE/dx$ distributions for both the electron-enriched and hadronic samples. The subtracted distribution together with the background from the photon conversions are shown in Fig. 5b. Similar distributions are seen in the individual bins of $p_T^{\text{trk}}$ and $\eta^{\text{trk}}$. In Fig. 5a, the two distributions have the same shape for $dE/dx$ values below $\sim 1.1$ mips, but there is a clear excess of the electron-enriched sample over the hadronic sample at larger values of $dE/dx$, indicating the presence of electrons. The excess over the conversion signal was used to extract cross sections for electrons from heavy-quark decays. A cut at the mean value for electrons of $dE/dx = 1.4$ mips was made, which, assuming a symmetrical Gaussian distribution (as suggested by Fig. 2a), has an efficiency of 50%. Varying the cut in steps of 0.01 mips between 1.3 and 1.5 mips gave the same results within the statistical uncertainties. Cutting at lower values of $dE/dx$ gave no overall improvement in the statistical error.

The number of identified electrons after this procedure is $1480 \pm 63$, of which $537 \pm 29$ were attributed to photons converting into electron-positron pairs, resulting in $943 \pm 69$ electrons used for the cross section determination. The same statistical subtraction procedure was used in each bin to extract the differential cross sections.

5

# 4 Monte Carlo event simulation

The acceptance and the effects of detector response were determined using samples of MC events. The programs HERWIG 5.9 [23] and PYTHIA 5.7 [24], which implement the leading-order matrix elements followed by parton showers, were used. For all generated events, the ZEUS detector response was simulated in detail using a program based on GEANT3.13 [25].

At leading order (LO), two types of processes can be distinguished: direct photon processes, in which the photon couples directly to a parton in the proton; and resolved photon processes, where the photon acts as a source of partons, one of which participates in the hard interaction. Samples of direct and resolved photon events, including heavy-quark excitation processes, were generated separately. For acceptance corrections, the MC events were generated with the CTEQ-4D [26] structure function for the proton and GRV-LO [27] for the photon. The default quark masses were used in both HERWIG and PYTHIA.

For the fitting procedure and MC predictions, the GRV94-LO structure function for the proton and the GRV-LO for the photon were used. The quark masses were set to the nominal values of $m_b = 4.75$ GeV and $m_c = 1.5$ GeV. Samples with different input parton density functions and different quark masses were used to evaluate systematic effects.

Both the shape and normalisation of the MC samples were compared to the differential cross sections. Fits to the data yielded the fraction of resolved photon processes as well as of beauty production. The cross-section value predicted by the MC model was also compared to the measured $b \rightarrow e^-$ cross section. The MC predictions were then used to extrapolate the measured cross section to the parton level to facilitate a comparison with an NLO calculation.

# 5 Event characteristics

Comparisons of the distributions of kinematic quantities between the data and the HERWIG and PYTHIA MC simulations, which include production of all five flavours of quark, are shown in Fig. 6. Both MC models describe the data reasonably well.

The number of jets is more accurately described by the PYTHIA MC but the jet quantities themselves are well described by both MC programs. The general shape of the $p_T^{\mathrm{trk}}$ distribution is well described, although there are slightly more events in the data at high $p_T^{\mathrm{trk}}$. The matching of the track-cluster pairs is also well described, as demonstrated by the distribution of $d$, the distance of closest approach of the track and the cluster. The separation of the jet and electron candidate in $\eta - \phi$ space, $R_{\mathrm{e-jet}}$, is peaked at low values with a flat tail at $R_{\mathrm{e-jet}} > 1$, amounting to 10% of the sample; it is described reasonably by the MC programs. Confidence in the use of the MC programs for acceptance corrections was thus justified.

Also shown in Fig. 6 is the contribution in the MC model from the semi-leptonic decays of beauty quarks. These events, in general, have jets with larger transverse energy and have a tendency to be more forward (i.e. nearer to the proton beam direction) in $\eta^{\mathrm{jet}}$. The prompt electron is more separated from the jet, being produced with a higher transverse momentum and also in a more forward direction.

# 6 Cross section measurements

The signal for beauty decays can be seen in Fig. 7, in which the $p_T^{\text{rel}}$ distribution, where $p_T^{\text{rel}}$ is the momentum of the electron transverse to the axis of the jet to which it is closest, is compared to the MC prediction. The data peak at low $p_T^{\text{rel}}$, consistent with predominantly semi-leptonic decays of charm quarks, with other contributions mostly from $\tau$ and $\eta$ decays contributing less than 3%. At high $p_T^{\text{rel}}$, the data fall less steeply than the predictions for charm. The data are consistent with a significant contribution from $b$ decays.

## 6.1 Differential cross sections

Differential cross sections were determined as a function of $p_T^{\text{rel}}$ and $x_\gamma^{\text{obs}}$, the fraction of the photon's momentum contributing to the production of the two highest transverse energy $(E_T^{\text{jet}})$ jets. The variable $x_\gamma^{\text{obs}}$ is defined as [28]:

$$x_\gamma^{\text{obs}} = \frac{\sum_{\text{jets}} E_T^{\text{jet}} e^{-\eta^{\text{jet}}}}{2yE_e}, \tag{2}$$

where the sum is over the two jets of highest transverse energy. Cross sections for reaction (1) were measured in a restricted kinematic region with $p_T^{e^-} > 1.6$ GeV and $|\eta^{e^-}| < 1.1$. Differential electron cross sections, $d\sigma/dp_T^{\text{rel}}$ and $d\sigma/dx_\gamma^{\text{obs}}$, were determined in the region $Q^2 < 1$ GeV$^2$, $0.2 < y < 0.8$, requiring events with at least two jets with $E_T^{\text{jet1(2)}} > 7(6)$ GeV and $|\eta^{\text{jet}}| < 2.4$. For a given luminosity, $\mathcal{L}$, the cross section, $\sigma_i$, in bin $i$ is given by $\sigma_i = N_i^{\text{corr}} / (\mathcal{L} \cdot \Delta)$, where $N_i^{\text{corr}}$ is the acceptance-corrected number of electrons in the bin $i$ and $\Delta$ is the bin width. The acceptance correction-factors were obtained from MC simulations using a bin-by-bin method. The reference MC model was HERWIG, with PYTHIA used as a systematic check. At low $p_T^{\text{rel}}$, the value of the correction factor was 2.3, decreasing with increasing values of $p_T^{\text{rel}}$ to a minimum of 0.8. For the cross section as a function of $x_\gamma^{\text{obs}}$, the correction factors were in the range $1.1 - 2.7$, increasing with increasing $x_\gamma^{\text{obs}}$.

The measured differential cross sections, $d\sigma/dp_T^{\text{rel}}$ and $d\sigma/dx_\gamma^{\text{obs}}$, where the $e^-$ comes from the semi-leptonic decay of a heavy quark, are shown in Figs. 7 and 8 respectively. The contribution from Dalitz decays was removed via the procedure and with the efficiency estimated in Section 3.2.5. The data are compared to the expectations of the HERWIG MC simulation, which was area normalised to the data for a comparison of shape; the scaling factor was 3.8.

Figure 8 shows a peak at high $x_\gamma^{\text{obs}}$, consistent with direct photon processes. However, the tail at low $x_\gamma^{\text{obs}}$ cannot be explained by direct processes alone. The HERWIG prediction of 35% resolved photon contribution (including flavour-excitation processes) and 65% direct gives good agreement with the data. Fitting the shape of the direct and resolved photon MC distributions to the data gave a resolved component of $28\pm5(stat.)\%$ ($\chi^2/\text{ndf} = 1.5$). It can therefore be concluded that LO MC models require resolved photon processes to describe heavy quark production, as was observed in the ZEUS result for charm [1].

## 6.2 Beauty cross section

The beauty cross section was extracted by fitting the $p_T^{\text{rel}}$ distribution of the data to the sum of contributions from beauty and charm. In the fit, the relative fraction of beauty and charm in the MC simulation was varied and the fraction of beauty processes in the kinematic region was extracted by minimising $\chi^2$. The quoted beauty cross section below includes only the direct semileptonic decay from a $b$ quark to an electron since the cascade decay, $\bar{b} \rightarrow \bar{c} \rightarrow e^-$ is included in the background expected from charm because it exhibits a $p_T^{\text{rel}}$ spectrum more similar to a charm than a beauty decay.

The percentage of beauty production was determined to be $14.7 \pm 3.8$ (*stat.*) % ($\chi^2$/ndf $= 1.1$). Using this, the cross section for beauty production in the restricted kinematic region: $Q^2 < 1 \text{ GeV}^2$, $0.2 < y < 0.8$, with at least two jets, $E_T^{\text{jet1(2)}} > 7(6)$ GeV and $|\eta^{\text{jet}}| < 2.4$ and a prompt electron with $p_T^{e^-} > 1.6$ GeV and $|\eta^{e^-}| < 1.1$, was found to be

$$\sigma^{b \rightarrow e^-}_{e^+ p \rightarrow e^+ + \text{dijet} + e^- + X} = 24.9 \pm 6.4^{+4.2}_{-7.3} \text{ pb}. \tag{3}$$

The predictions from the two MC models are 8 pb for HERWIG and 18 pb for PYTHIA, using the parameter settings quoted in Section 4 for the fitting procedure. The large difference in the MC predictions comes mainly from the different default treatments of $\alpha_s$, different scales and hadronisation and the use of massive matrix elements in HERWIG [23] and massless in PYTHIA [24] for the generation of flavour-excitation processes. Despite the cross-section differences, the predicted fractions of beauty production are 16.2% in HERWIG and 19.5% in PYTHIA, both in reasonable agreement with the data value of $14.7 \pm 3.8$ (*stat.*) %. Using the same procedure for charm, the measured cross section was found to be in reasonable agreement with the ZEUS measurement of $D^*$ production [1].

## 6.3 Systematic uncertainties

A detailed study of possible sources of systematic uncertainty was performed for the differential and total cross-section measurements by varying cuts on the quantities to check the acceptance and by using the alternative MC model to check the stability of the fit. The largest contributions to the systematic error for the differential cross sections $d\sigma/dp_T^{\text{rel}}$ and $d\sigma/dx_\gamma^{\text{obs}}$ were due to the uncertainty in the CAL energy scale and the use of PYTHIA instead of HERWIG to correct the data. In the case of the measured beauty total cross section, the significant errors were:

- using PYTHIA instead of HERWIG gave an uncertainty of $-8\%$;

- the range for $y_{JB}$ was varied by the resolution of 8%, leading to an uncertainty of $^{+0}_{-11}\%$;

- requiring $R_{\text{e-jet}} < 2$ rather than no requirement gave an uncertainty of $-10\%$.

- the normalisation range of the hadronic background to the electron-enriched sample was changed to $0.5 < dE/dx < 1.04$ mips, changing the cross section by $-12\%$.

- varying the distance of closest approach of the track-cluster pair, $d$, by $\pm 5$ cm changed the cross section by $^{+7}_{-3}\%$.

- varying the cuts for the hadronic sample on the fraction $E_{\rm EMC}/E_{\rm TOT}$ between 0.3 and 0.5 and for the electron-enriched sample between $E_{\rm EMC}/E_{\rm TOT} > 0.85$ and 0.95 gave an uncertainty of $^{+13}_{-16}\%$.

- using the CTEQ-4L proton structure function yielded a systematic error of $-4\%$, while using the GS96-LO [29] photon structure function yielded a systematic error of $-5\%$.

All systematic uncertainties on the differential cross sections, excluding the correlated uncertainties due to the luminosity and hadronic energy scale, were added in quadrature. For the total cross section, all systematic uncertainties except that due to the luminosity were added in quadrature.

# 7 Extrapolation to parton level cross section

## 7.1 Extrapolation procedure

The measured beauty cross section was extrapolated to the parton level in a restricted range of the transverse momentum and pseudorapidity of the beauty quark using the two MC models. The region in pseudorapidity for the beauty quark was defined such that the acceptance was reasonably constant over the range considered. The MC simulation predicts that 95% of events used in the cross-section determination of Eq. (3) have a $b$-quark of transverse momentum $p_T^b > 5$ GeV. Accordingly, the measured cross section was extrapolated to the parton level for the region $p_T^b > p_T^{\rm min} = 5$ GeV, $|\eta^b| < 2$, $Q^2 < 1$ GeV$^2$ and $0.2 < y < 0.8$. The extrapolation factor $f_{\rm ext}$ is then given by

$$ f_{\rm ext} = \left[ \frac{\sigma_{e^+p \to e^+bX}^{b \to e^-}}{\sigma_{e^+p \to e^+ + {\rm dijet} + e^- + X}^{b \to e^-}} \right]_{\rm MC} . $$

The value obtained using the HERWIG MC generator was $f_{\rm ext} = 6.8$. To correct to the full $b$ cross section the branching ratio for the process of $b \to e^-$ (10.73 $\pm$ 0.35) % [20] was used. The major source of uncertainty on the extrapolation factor arises from the uncertainty in the hadronisation, quantified by the use of PYTHIA, to be -26%; PYTHIA uses the Lund model while HERWIG uses the cluster model. The other significant sources of uncertainty arise from varying the space-like evolution parameters[3] ($-11\%$), varying the mass of the $b$ quark from 4.5 GeV to 5.0 GeV ($^{+8}_{-2}\%$) and the branching ratio ($\pm 3\%$). Applying $f_{\rm ext}$ and the branching ratio to the measured cross section gives

$$ \sigma_{ep \to e^+bX}^{\rm ext} = 1.6 \pm 0.4(stat.)^{+0.3}_{-0.5}(syst.)^{+0.2}_{-0.4}(ext.) \text{ nb} $$

where the last error given is the estimate for the error arising from the extrapolation procedure.

## 7.2 Comparison with NLO predictions

The cross section is compared in Fig. 9 to a NLO QCD calculation [30]. The prediction comes from a fixed-order calculation in which $b$ quarks are not active partons in the proton and photon

---

[3]For the central analysis, the default setting, denoted by the variable `ISPAC = 0`, allows the backward evolution down to some cut-off, `QSPAC`, which was set to 1 GeV. By changing to `ISPAC = 1`, the backward evolution continues to the infra-red cut-off, but the parton density functions are frozen at the value `QSPAC`, which is again set to 1 GeV.

structure functions and are generated dynamically in the hard sub-process. The NLO calculation uses the MRST99 [31] and GRV-G HO [27] parton-density parametrisations for the proton and photon, respectively. For the central prediction, the renormalisation and factorisation scales are set to the transverse mass, $\mu_R = \mu_F = m_T = \sqrt{m_b^2 + p_T^2}$, where $m_b = 4.75$ GeV. The predicted cross section in the region $p_T^b > 5$ GeV, $|\eta^b| < 2$, $Q^2 < 1$ GeV$^2$ and $0.2 < y < 0.8$ for the above settings is 0.64 nb. The values produced by variation of the mass of the beauty quark (4.5 and 5.0 GeV) and the renormalisation and factorisation scales ($2m_T$ and $m_T/2$) are shown in Fig. 9 as the upper and lower predictions. Using other sets of parton density functions, e.g. MRST99 ($g \downarrow$), MRST99 ($g \uparrow$), MRST99($\alpha_s \downarrow\downarrow$) and MRST99($\alpha_s \uparrow\uparrow$), in which the extremes of an allowed range of values are taken [31], resulted in variations of the NLO predictions for $p_T^{\min} > 5$ GeV of within $\pm 4\%$. Using CTEQ 5M1 [32] and GRV98 HO [33] proton structure functions changes the prediction by +2% and −5%, respectively.

The extrapolated cross section lies somewhat above the central NLO prediction, consistent with the general observation that NLO QCD calculations underestimate beauty production both in hadroproduction [4, 5, 6] and photoproduction at HERA [3].

# 8   Summary

The production and semi-leptonic decay of heavy quarks has been studied in the photoproduction process $e^+p \rightarrow e^+ + \text{dijet} + e^- + X$ with the ZEUS detector at HERA using an integrated luminosity of 38.5 pb$^{-1}$. Events with photon-proton centre-of-mass energies, $W_{\gamma p}$, in the range $134 < W_{\gamma p} < 269$ GeV and a photon virtuality, $Q^2 < 1$ GeV$^2$, were selected with at least two jets of transverse energy $E_T^{\text{jet1(2)}} > 7(6)$ GeV and an electron in the final state. The beauty cross section was measured to be $\sigma_{e^+p \rightarrow e^+ + \text{dijet} + e^- + X}^{b \rightarrow e^-} = 24.9 \pm 6.4^{+4.2}_{-7.3}$ pb. This cross section was extrapolated to the parton level with a $b$ quark restricted to the region of transverse momentum $p_T^b > 5$ GeV and pseudorapidity $|\eta^b| < 2$ for the events with $Q^2 < 1$ GeV$^2$ and $0.2 < y < 0.8$. The value obtained, $\sigma_{ep \rightarrow e^+bX}^{\text{ext}} = 1.6 \pm 0.4 \, (stat.) \, ^{+0.3}_{-0.5}(syst.)^{+0.2}_{-0.4}(ext.)$ nb, lies somewhat above the NLO predictions, in agreement with results both from hadroproduction and photoproduction.

# Acknowledgements

# References

[1] ZEUS Collaboration, J. Breitweg et al., Eur. Phys. J. C**6** 67 (1999)

[2] H1 Collaboration, C. Adloff et al., Nucl. Phys. B**545** 21 (1999)

[3] H1 Collaboration, C. Adloff et al., Phys. Lett. B**467** 156 (1999)

[4] UA1 Collaboration, C. Albajar et al., Phys. Lett. B**256** 121 (1991)
*erratum:*
UA1 Collaboration, C. Albajar et al., Phys. Lett. B**262** 497 (1991)

[5] CDF Collaboration, F. Abe et al., Phys. Rev. Lett. **68** 3403 (1992);
CDF Collaboration, F. Abe et al., Phys. Rev. Lett. **69** 3704 (1992);
CDF Collaboration, F. Abe et al., Phys. Rev. Lett. **71** 500 (1993);
CDF Collaboration, F. Abe et al., Phys. Rev. Lett. **71** 2396 (1993);
CDF Collaboration, F. Abe et al., Phys. Rev. Lett. **71** 2537 (1993);
CDF Collaboration, F. Abe et al., Phys. Rev. D**50** 4252 (1994)

[6] D0 Collaboration, S. Abachi et al., Phys. Rev. Lett. **74** 3548 (1995);
D0 Collaboration, S. Abachi et al., Phys. Lett. B**370** 239 (1996)

[7] ZEUS Collaboration, M. Derrick et al., Phys. Lett. B**293** 465 (1992)

[8] The ZEUS Detector, Status Report 1993, DESY 1993

[9] N. Harnew et al., Nucl. Instrum. Methods A**279** 290 (1989);
B. Foster et al., Nucl. Phys., Proc-Suppl. B**32** 181 (1993);
B. Foster et al., Nucl. Instrum. Methods A**338** 254 (1994)

[10] O. Deppe, "Measurement of $D^{*\pm}$ Electroproduction at HERA", Ph.D. Thesis, DESY, (2000) DESY-THESIS-2000-006.

[11] M. Derrick et al., Nucl. Instrum. Methods A**309** 77 (1991);
A. Andresen et al., Nucl. Instrum. Methods A**309** 101 (1991);
A. Bernstein et al., Nucl. Instrum. Methods A**336** 23 (1993)

[12] J. Andruszków et al., DESY 92-066 (1992);
ZEUS Collaboration, M. Derrick et al., Z. Phys. C**63** 391 (1994)

[13] ZEUS Collaboration, J. Breitweg et al., Eur. Phys. J. C**1** 109 (1998)

[14] ZEUS Collaboration, M. Derrick et al., Phys. Lett. B**322** 287 (1994)

[15] F. Jacquet and A. Blondel, in "Proceedings of The Study for an *ep* Facility for Europe", ed. U. Amaldi, (DESY 79/48 1979), 391

[16] S. Catani et al., Nucl. Phys. B**406** 187 (1993)

[17] S. D. Ellis and D. E. Soper, Phys. Rev. D**48** 3160 (1993)

[18] R. van Woudenberg, "Study of Charm Production at HERA using the ZEUS Detector", Ph. D. Thesis, University of Amsterdam, (1995) (unpublished);
W. Verkerke, "Measurement of Charm Production in Deep Inelastic Scattering", Ph. D. Thesis, University of Amsterdam, (1998) (unpublished);
K. Hebbel, "Measurement of Charm Production in Deep Inelastic *ep* Scattering at HERA", Ph.D. Thesis, DESY, (2000) DESY-THESIS-2000-016.

[19] M. Wing, "The Study of Heavy Quark Production in High $E_T$ Photoproduction at HERA using the ZEUS Detector.", Ph.D. Thesis, UCL (1999), RAL-TH-1999-011 (unpublished)

[20] D.E. Groom et al., Eur. Phys. J. C**15** 1 (2000)

[21] R. W. Hendricks, Rev. Sci. Inst. **40** 1216 (1969)

[22] Y-S Tsai, Rev. Mod. Phys. **46** 815 (1974);
*erratum:*
Y-S Tsai, Rev. Mod. Phys. **49** 421 (1977)

[23] G. Marchesini et al., Comp. Phys. Commun. **67** 465 (1992)

[24] H.-U. Bengtsson and T. Sjöstrand, Comp. Phys. Commun. **46** 43 (1987)

[25] GEANT 3.13, R. Brun et al., CERN/DD/EE/84-1 (1987)

[26] H. L. Lai et al., Phys. Rev. D**55** 1280 (1997).

[27] M. Glück, E. Reya and A. Vogt, Phys. Rev. D**45** 3986 (1992);
M. Glück, E. Reya and A. Vogt, Phys. Rev. D**46** 1973 (1992)

[28] ZEUS Collaboration, M. Derrick et al., Phys. Lett. B**348** 665 (1995)

[29] L. E. Gordon and J. K. Storrow, Nucl. Phys. B**489** 405 (1997)

[30] S. Frixione et al., Phys. Lett. **348** 633 (1995);
S. Frixione et al., Nucl. Phys. B**454** 3 (1995)

[31] A. D. Martin et al., Eur. Phys. J. C**4** 463 (1998);
A. D. Martin et al., Eur. Phys. J. C**14** 133 (2000)

[32] CTEQ Collaboration, H. L. Lai et al., Eur. Phys. J. C**12** 375 (2000)

[33] M. Glück, E. Reya and A. Vogt, Eur. Phys. J. C**5** 461 (1998)

[34] H. A. Bethe, Ann. Phys. **5** 325 (1930);
H. A. Bethe, Z. Phys. **76** 293 (1932);
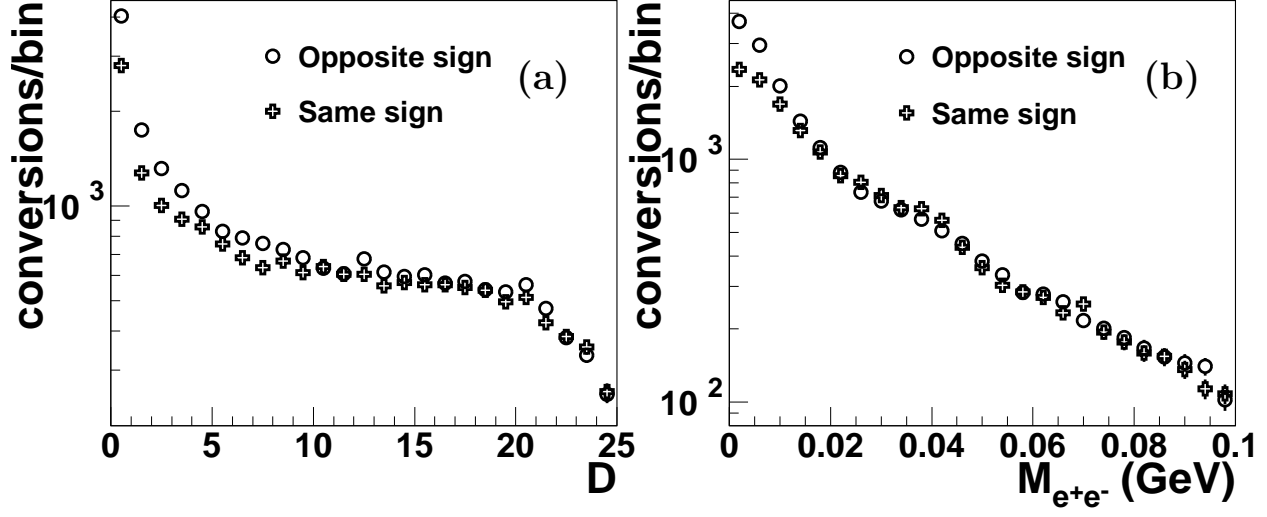F. Bloch, Ann. Phys. **16** 285 (1933).

Figure 1: (a) The distribution of the quality factor, $D$, (see Section 3.2.2) for conversion candidates. (b) the invariant mass, $M_{e^+e^-}$, for conversion candidates. In (a) and (b), the conversion candidates resulting in pairs with zero net charge are shown as points; those pairs having non-zero net charge are shown as the crosses.
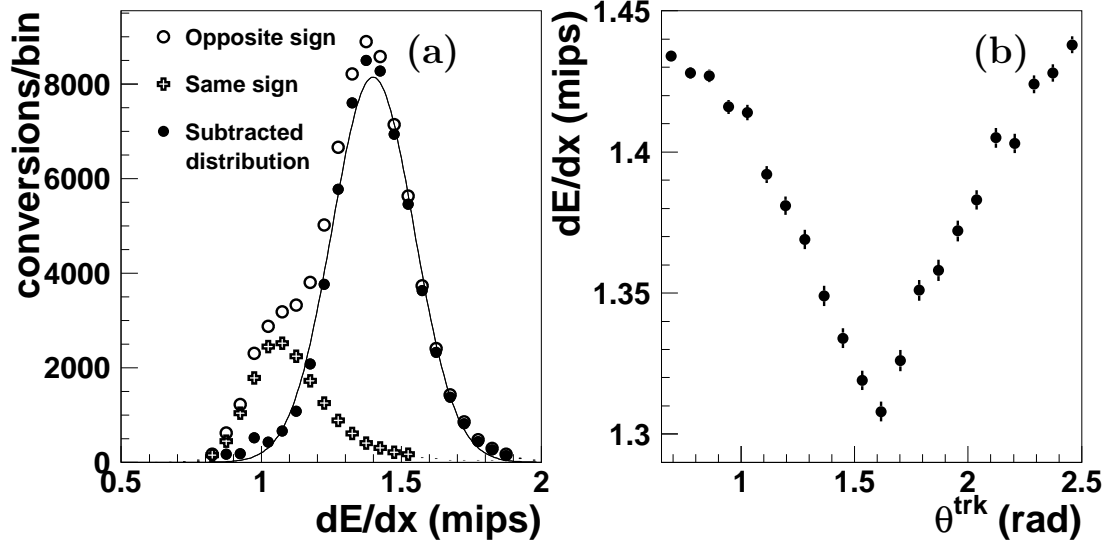
Figure 2: (a) The $dE/dx$ distribution of photon-conversion candidates and (b) the dependence on the polar angle, $\theta^{\mathrm{trk}}$, for electrons. In (a), photon-conversion candidates having two tracks of opposite charge are shown as open circles whereas those with tracks of the same sign are shown as the crosses; the solid circles show the difference between these two distributions. A Gaussian fit is shown in (a) for illustration.
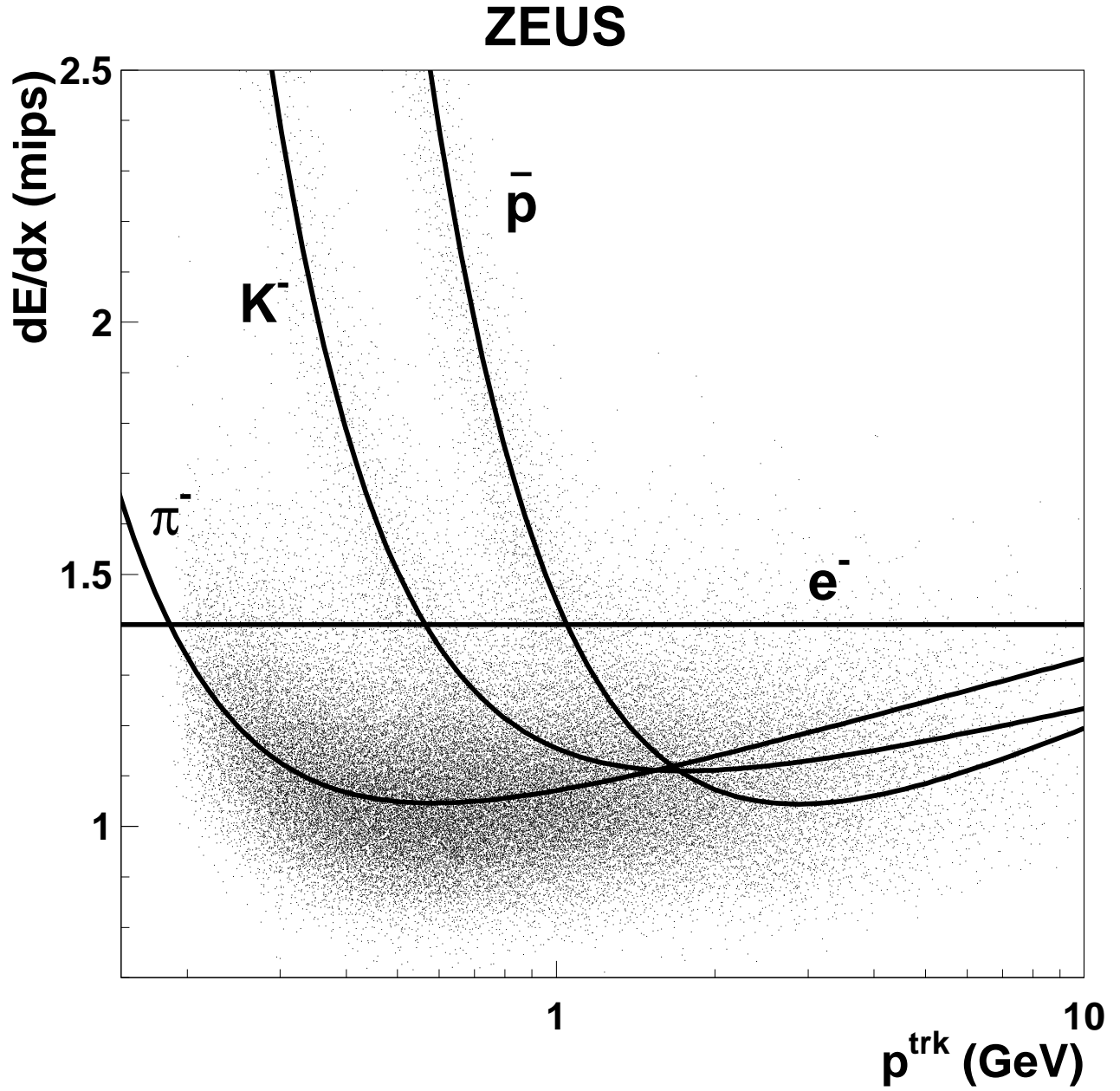
Figure 3: The measured distribution of $dE/dx$ against momentum, $p^{\mathrm{trk}}$, for negative tracks in the range $|\eta^{\mathrm{trk}}| < 1.1$, as for the analysis. The curves show the expected average values for particular types of particles as derived from the Bethe-Bloch formula [34]. The events are a sub-sample of those that pass the dijet trigger requirements.
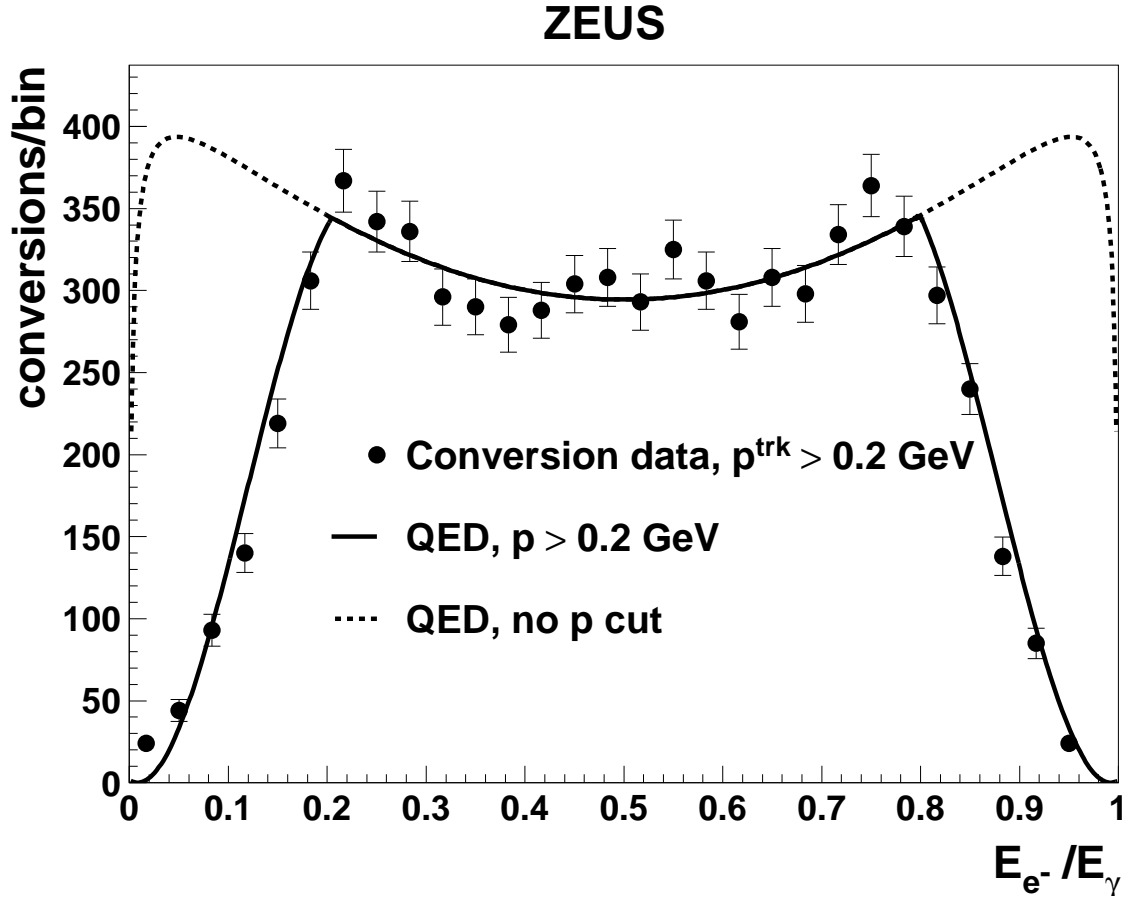
Figure 4: Comparison of the number of electrons found in the data (points) with the prediction from pair production (solid line) for conversions in which both tracks have a momentum greater than 0.2 GeV. The prediction for no cut on the momentum of the tracks is also shown as the dashed line.
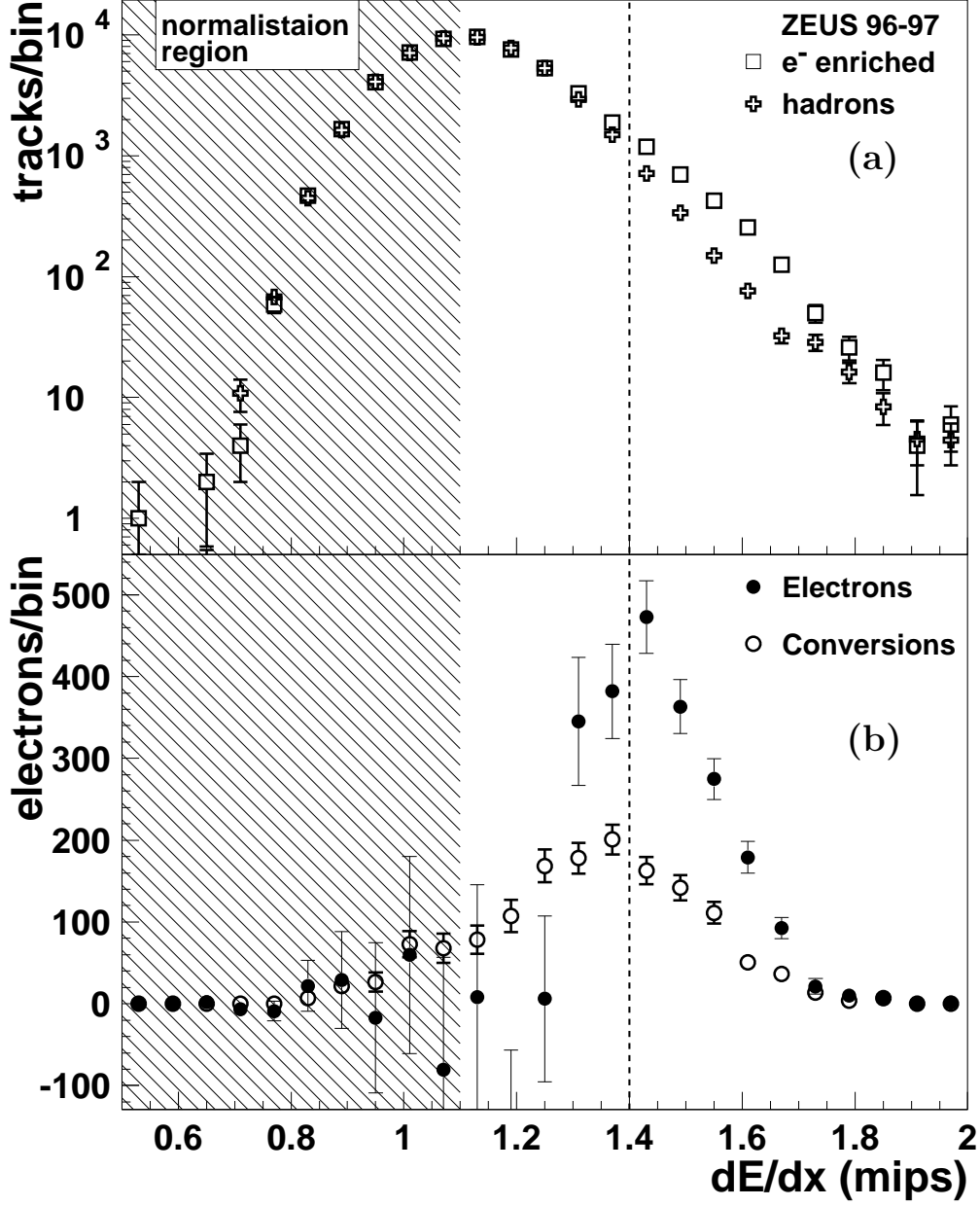
**ZEUS**



Figure 5: (a) The $dE/dx$ distribution for the hadronic sample (crosses) and electron-enriched (open squares) sample normalised to each other in the hatched region shown. (b) The difference between the electron-enriched and hadronic samples (solid circles), together with the background arising from photon conversions (open circles). The data in the region with $dE/dx > 1.4$ mips shown by the dashed line were used to extract the results in this paper.
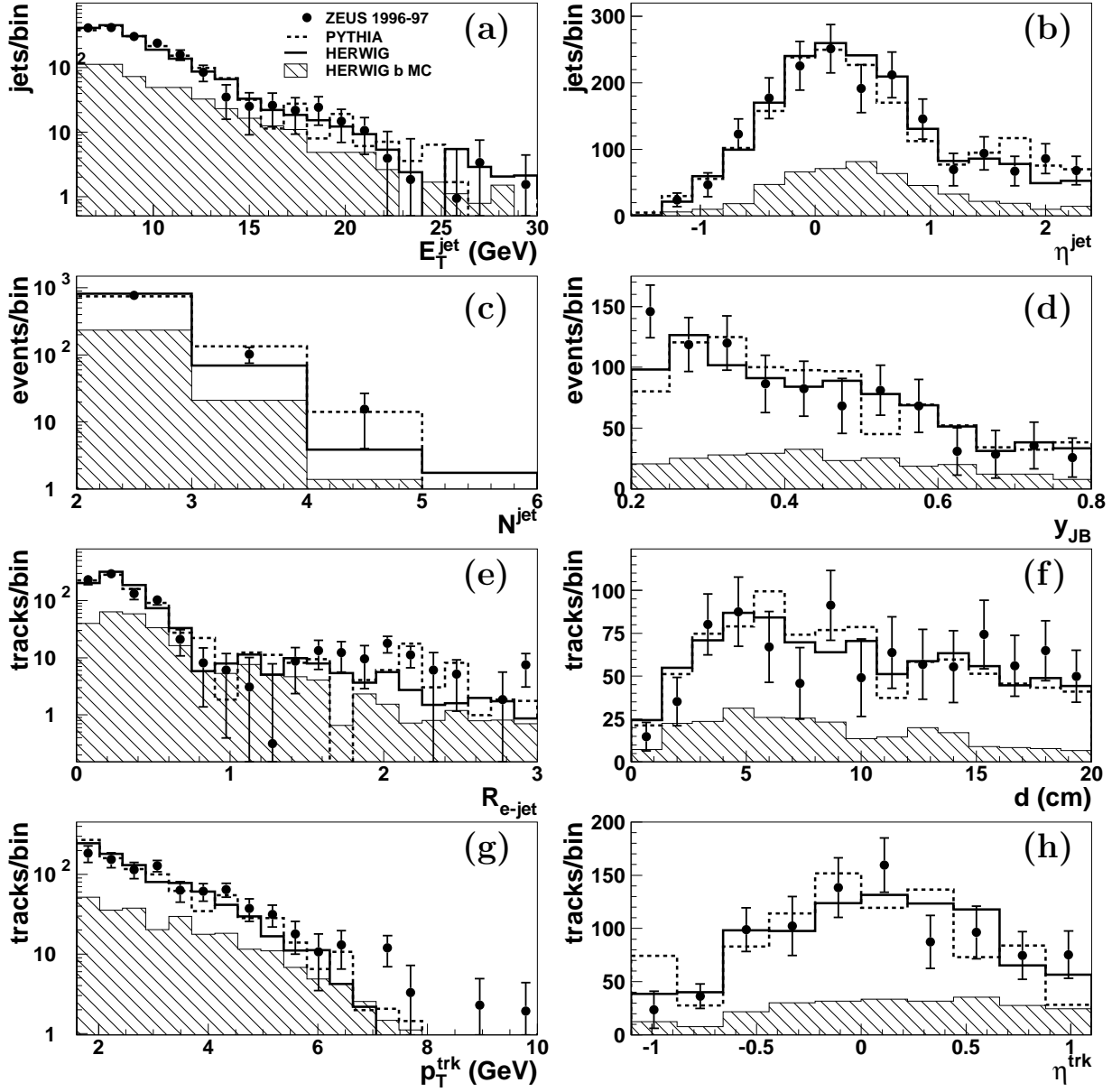
**ZEUS**



Figure 6: Comparison of data (points) with HERWIG (solid line) and PYTHIA (dashed line) MC expectations for: (a) jet transverse energy, $E_T^{\text{jet}}$; (b) pseudorapidity of the jet, $\eta^{\text{jet}}$; (c) number of jets in the event, $N^{\text{jet}}$; (d) the Jacquet-Blondel estimator of $y$, $y_{\text{JB}}$; (e) the separation of the electron track and jet, $R_{\text{e-jet}}$; (f) the distance of closest approach of the track-cluster pair, $d$; (g) the transverse momentum of the track, $p_T^{\text{trk}}$, and (h) the pseudorapidity of the track, $\eta^{\text{trk}}$. The MC prediction is area normalised to the number of data events. The contribution of events with an electron from the semi-leptonic decay of a $b$ quark to the MC prediction is shown as the hatched histogram. The normalisation for the MC from $b$-decays is the same as for the total sample and the fraction is that predicted in HERWIG.
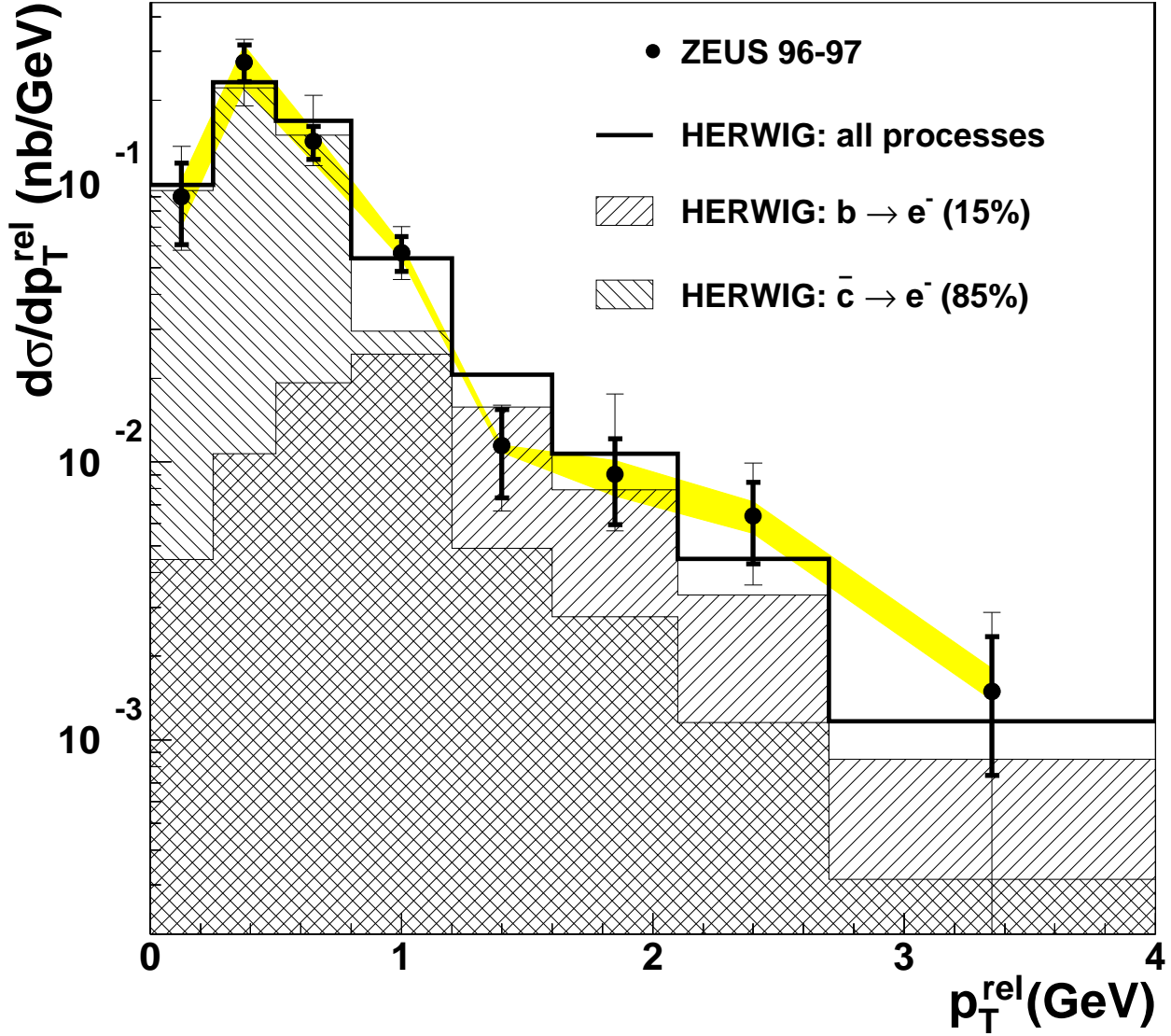
18

Figure 7: The differential cross-section $d\sigma/dp_T^{\mathrm{rel}}$ for heavy quark decays. The inner error bars represent statistical errors and the outer bars statistical and systematic errors added in quadrature. The effect of the energy scale uncertainty is shown as the shaded band. The experimental data is compared to the HERWIG MC prediction (solid line) for all quark flavours, which has been fitted to the data and scaled up by a factor of 3.8. The components from the beauty processes (forward-diagonally hatched histogram) and from charm (backward-diagonally hatched histogram) predicted by the HERWIG MC model are indicated separately.
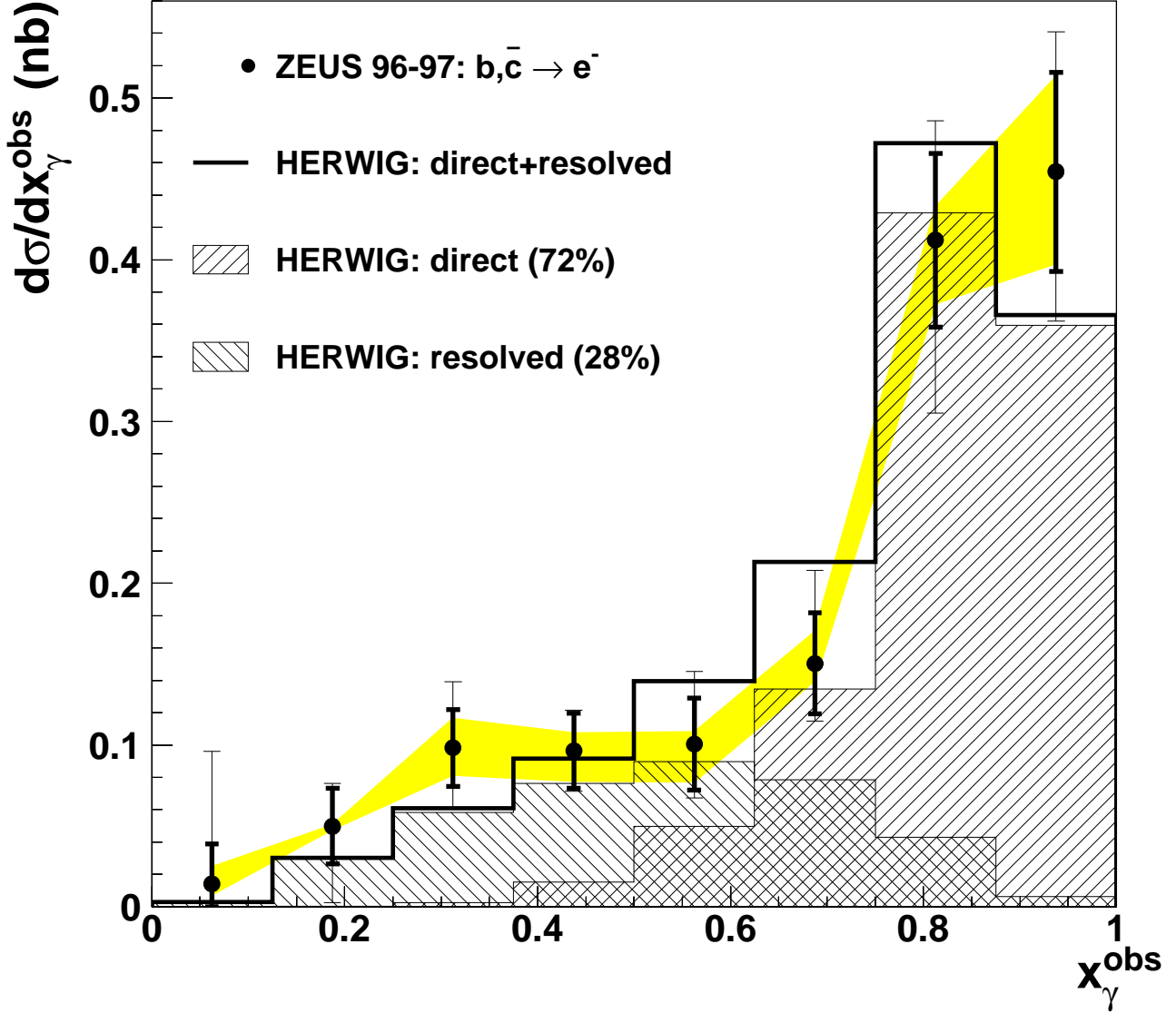
# ZEUS



Figure 8: The differential cross-section $d\sigma/dx_\gamma^{\mathrm{obs}}$ for heavy quark decays. The inner error bars represent statistical errors and the outer bars statistical and systematic errors added in quadrature. The effect of the energy scale uncertainty is shown as the shaded band. The experimental data is compared to the HERWIG MC prediction (solid line) for all quark flavours, which has been fitted to the data and scaled up by a factor of 3.8. The direct (forward-diagonally hatched histogram) and resolved photon components (backward-diagonally hatched histogram) are indicated separately.
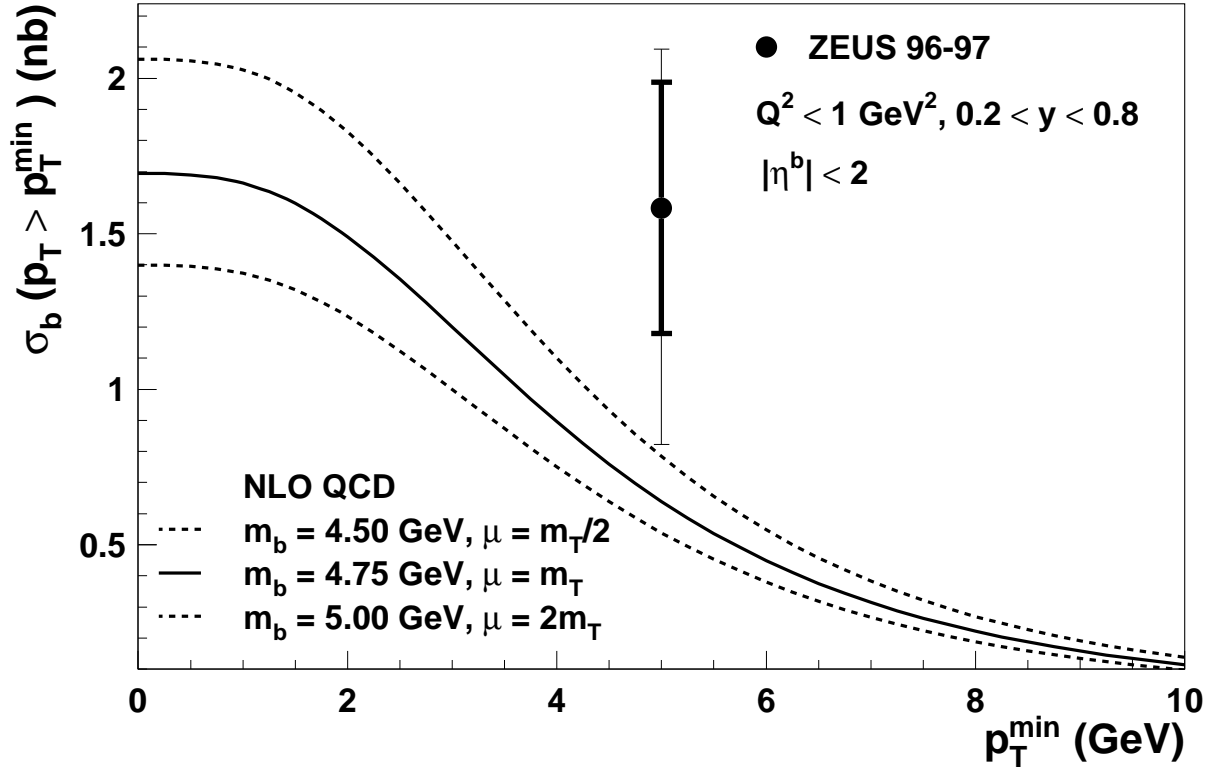
20

**ZEUS**

Figure 9: The extrapolated $b$ cross section at a fixed $p_T^{\min}$ value compared with theoretical predictions plotted as a function of $p_T^{\min}$. The inner error bars represent the statistical error and the outer bars statistical, systematic and extrapolation errors added in quadrature. The curves show the predictions from NLO QCD for varying $b$-quark mass and varying factorisation and renormalisation scale $m_T = \sqrt{m_b^2 + p_T^2}$.